

# Electronic, Magnetic, and Elastic Features of Quaternary Heusler Alloys: FeVScSb and FeVYSb

Ilhem Bensehil, Hakim Baaziz,\* Torkia Ghellab, Zoulikha Charifi, Ahlem Kolli, and Nacir Guechi

This study employs density functional theory to investigate the structural, elastic, electronic, and magnetic properties of FeVScSb and FeVYSb Heusler compounds. FeVScSb exhibits ferromagnetic properties in its stable state, whereas FeVYSb displays ferrimagnetic behavior. The obtained elastic constants ( $C_{ij}$ ) indicate that FeVScSb and FeVYSb possess mechanical stability and ductility, while also displaying a significant degree of elastic anisotropy. The aggregate magnetic moment of said alloys is determined to be equivalent to  $3 \mu_B$ , in accordance with the Slater–Pauling principle. The investigation of the impact of uniform strain on electronic and magnetic characteristics is conducted. The findings indicate that FeVScSb and FeVYSb exhibit semiconductivity within extensive lattice parameter intervals, ranging from 5.84 to 6.60 Å for FeVScSb and from 6.11 to 6.70 Å for FeVYSb. The Heusler compounds FeVScSb and FeVYSb exhibit half-metallic behavior within a range of lattice parameters. Specifically, FeVScSb displays this behavior when the lattice parameter varies from 6.61 to 6.72 Å, while FeVYSb exhibits half-metallicity within the range of 6.71–6.81 Å. Under the influence of strain, the magnetic moment retains a constant value of  $3 \mu_B$ . Therefore, the potential for spintronics is promising.

## 1. Introduction

The field of spintronics is currently a leading area of investigation in the realm of novel materials exhibiting unconventional properties, which can be attributed to the rapid advancement of nanoscience.<sup>[1]</sup> The potential of utilizing high-spin-polarization materials in the field of spintronics has generated significant attention among researchers.<sup>[2,3]</sup> Heusler compounds have been extensively researched due to their high Curie temperature, 100% spin polarization, and tunable electronic characteristics.<sup>[4–7]</sup> Heusler alloys can be classified into two distinct categories, namely, half-Heusler and full-Heusler compounds. The chemical entities denoted as X, X', Y, and Z belong to the categories of transition metals and main group members, respectively. The chemical formulas associated with these entities are XYZ, X<sub>2</sub>YZ, and XX'YZ. Each of the aforementioned chemical formulas exhibits X with a greater valence than X', and X' with a greater valence than Y. In 1983, de Groot et al.<sup>[8]</sup> conducted a study which first proposed that the NiMnSb half-Heusler alloy could exhibit half-metallicity. Since then, electronic structure simulations have revealed that many half-Heuslers with a C1<sub>b</sub> configuration and full-Heuslers with an L2<sub>1</sub> configuration exhibit half-metallic behavior.<sup>[9–13]</sup> Several publications<sup>[14–17]</sup> have shed light on the rule of Slater and Pauling, which establishes a connection between the electronic and magnetic features, and the process by which the gap in Heusler alloy is formed. In addition, ternary Heusler alloys (NiMnSb, Co<sub>2</sub>CrAl, CoMnGe, and Ni<sub>2</sub>MnGa) have been extensively examined<sup>[18–22]</sup> for the impact of lattice distortions on magnetic and electronic characteristics.

A recent hypothesis posited that compounds of the LiMgPdSn type may demonstrate characteristics of half-metallicity, as indicated by sources.<sup>[23,24]</sup> The Y-type solids are characterized by the space group  $F\bar{4}3m$ . The CoFeMnSi compound serves as a prototypical model and has been the subject of extensive investigation by numerous research groups.<sup>[25–27]</sup> Dai et al.<sup>[24]</sup> inferred that CoFeMnSi is likely to exhibit a half-metallic property based on the analysis of its XRD pattern and magnetic measurements. The crystal structure of CoFeMnSi was found to be similar to that of LiMgPdSb. The hypothesis that CoFeMnSi exhibits a half-metallic property has been corroborated by both experimental


I. Bensehil  
Faculty of Technology  
University of M'sila  
B.P.166, Ichbilia, 28000 M'sila, Algeria

I. Bensehil, A. Kolli, N. Guechi  
Laboratory of Surfaces and Interfaces Studies of Solid Materials  
University Ferhat Abbas of Setif 1  
19000 Setif, Algeria

H. Baaziz, T. Ghellab, Z. Charifi  
Laboratory of Physics and Chemistry of Materials  
University of M'sila  
28000 M'sila, Algeria  
E-mail: hakim.baaziz@univ-msila.dz

H. Baaziz, Z. Charifi  
Department of Physics  
Faculty of Science  
University of M'sila  
28000 M'sila, Algeria

N. Guechi  
Faculty of Medicine  
University Ferhat Abbas of Setif 1  
19000 Setif, Algeria

 The ORCID identification number(s) for the author(s) of this article can be found under <https://doi.org/10.1002/pssb.202300178>.

DOI: 10.1002/pssb.202300178

findings and density functional theory (DFT) computations.<sup>[28]</sup> The material has a magnetic saturation of  $3.7 \mu_B$  f.u.<sup>-1</sup> and a Curie temperature of 620 K.

Feng et al.<sup>[29]</sup> have reported that CoFeMnSi exhibits a high degree of stability in terms of half-metallicity, even when subjected to potential growth-induced disorders. In their study, Ozdoğan et al.<sup>[30]</sup> utilized ab initio calculations to examine a total of 60 quaternary Heusler alloys. Out of these, 41 were identified as half-metals, while 9 were classified as semiconductors. Notably, 8 of the semiconductors exhibited spin gapless behavior. The CoFeCrZ (where Z represents Al, Si, Ga, and Ge) compounds were synthesized by Gao et al. and were found to exhibit remarkable half-metallicity, as evidenced by the discovery of spin-down bandgaps of 0.16 and 0.28 eV.<sup>[31,32]</sup>

The study conducted by Kundu and co-workers examined two distinct quaternary Heusler series, namely, CoXMnSi and CoXFeSi, wherein X represents the fifth-row elements ranging from Y to Ag. The researchers have identified CoTeMnSi, CoRhMnSi, and CoZrFeSi as authentic half-metallic materials, while a few other substances exhibit characteristics that are indicative of their potential to be classified as such. Yan et al.<sup>[33]</sup> conducted research which indicates that ZrTiCrZ (where Z represents Al, Ga, In, Si, Ge, Sn) exhibit characteristics of heavy metals, whereas ZrTiCrZ alloys with Z representing Si, Ge, and Sn demonstrate semiconductor properties in relation to their electronic, magnetic, and mechanical attributes. All of the aforementioned alloys exhibit Curie temperatures ( $T_C$ ) that are higher than the ambient temperature when employing the mean field approximation (MFA).

Due to the difficulty in controlling strain during the experimental synthesis of quaternary Heusler alloys, research into their physical characteristics when subjected to external strain is essential. Researchers Wang et al.<sup>[34]</sup> investigated how uniform strain affected RuMnCrSb. Significant spin-down bandgaps are seen for uniform strain between -4% and 0, while  $E_F$  is inside this gap from -2% to 0%. Total magnetic moment of  $2 \mu_B$  and 100% spin polarization  $P$ , from 4% to 0% uniform strain, show that RuMnCrSb's ideal HM is retained throughout the interval. In contrast to ZrRhTiZ ( $Z = \text{Al, In}$ ), where anomalous spin flip occurs at strains of -1% and 1%, Ray et al.<sup>[35]</sup> found that half-metallic ferromagnetic behavior is maintained within a -2% to 2% strain. Xiong<sup>[36]</sup> showed that the half-metallicities of CoFeTiSi, CoFeTiAs, and CoFeVSb may be maintained at lattice constants as low as 7%, 5%, and 6%, respectively, when compared to their equilibrium lattices. We further show that, with the right amount of in-plane strain, CoFeTiSi, CoFeTiAs, and CoFeVSb retain their HM properties. Half-metallicity was found to be invariant throughout a broad range of lattice constants (6.24–6.96 Å for Al, 6.12 Å–6.87 Å for Ga, and 6.14–6.94 Å for In) by Rahmoune et al.<sup>[37]</sup>

There are still a multitude of quaternary alloys that have not been explored. To the best of our knowledge, there is a dearth of literature pertaining to investigations conducted on the quaternary Heusler alloys FeVScSb and FeVYSb. The present investigation employs first-principles simulations to examine the structural, electronic, elastic, and magnetic properties of FeVScSb and FeVYSb, wherein Sc denotes a 3d element and Y represents a 4d element. This study has conducted investigations on the impact

of uniform strain on the electronic and magnetic characteristics of FeVScSb and FeVYSb compounds.

## 2. Calculation Method

The pseudopotential plane wave technique uses DFT as its basis,<sup>[38]</sup> and CASTEP, a computer program, has integrated it.<sup>[39]</sup> This method was used to investigate the fundamental ground-state assets of the FeVScSb and FeVYSb quaternary compounds in addition to the influence of hydrostatic pressure on the electronic and magnetic properties of the compounds. In the parameterization of the Perdew–Burke–Ernzerhof model,<sup>[40]</sup> the exchange and correlation impacts were dealt with in a self-consistent manner by making use of the generalized gradient approximation (GGA) that is the industry standard. The valence electron states of Fe:  $3d^6 4s^2$ , V:  $3d^3 4s^2$ , Y:  $4d^1 5s^2$ , and Sc:  $3d^1 4s^2$  were all calculated using the Vanderbilt ultrasoft pseudopotential.<sup>[41]</sup> We used a 450 eV cutoff for the plane wave energy and a  $14 \times 14 \times 14$  k-point mesh over the Brillouin zone (BZ) in Monkhorst–Pack<sup>[42]</sup> for the structural optimization, and a  $30 \times 30 \times 30$  k-point mesh for the determination of the density of states. Crystalline Heuslers FeVScSb and FeVYSb were also optimized using the Broyden–Fletcher–Goldfarb–Shanno minimization approach,<sup>[43]</sup> with a total energy convergence criterion of  $5 \times 10^{-6}$  eV atom<sup>-1</sup>. The band-energy structures were computed with 0.005 Å<sup>-1</sup>. The energy gap between successive repetitions of the atomic positions was relaxed until it was less than  $1 \times 10^{-6}$  eV atom<sup>-1</sup>. Limits of 0.002 eV Å<sup>-1</sup> for force and  $1 \times 10^{-4}$  Å for displacement were imposed. The stress–strain method<sup>[44]</sup> was utilized to ascertain the elastic constants ( $C_{ij}$ ). The Voigt–Reuss–Hill approaches<sup>[45–47]</sup> were used to predict the elastic moduli.

## 3. Results and Discussion

### 3.1. Structural Properties

Heusler alloys of both quaternary FeVScSb and FeVYSb form cubic crystals of the LiMgPdSn (Y-type) phase (space group  $F\bar{4}3m$ ).<sup>[48–52]</sup> This structure has three possible nonequivalent superstructures (YI, YII, and YIII) summarized in Table 1. In both FeVScSb and FeVYSb Heuslers, the three possible nonequivalent atomic arrangements (YI, YII, and YIII) are shown in Figure 1. A stability of a structural phase at zero temperature and pressure investigation was performed to identify the ground-state properties of FeVScSb and FeVYSb Heuslers by taking into account both the ferromagnetic and paramagnetic arrangements of each atom inside the conventional cell. While discussing magnetic states, both ferromagnetic and ferrimagnetic orders of spins are included. It is worth noting that the CASTEP algorithm optimizes electron spin in addition to geometric parameters. By varying the lattice parameter ( $a$ ) from 5.83 to 6.85 Å in increments of 0.127 Å for FeVScSb (FeVYSb), we were successful in optimizing the crystal structures of FeVScSb and FeVYSb Heuslers by performing a total energy calculation for each of the three possible arrangements in structure (YI, YII, and YIII). Figure 1 shows the relationship between the computed total energy and the unit cell volume for both materials

**Table 1.** Three FeVScSb and FeVYSb Heusler compound sites in Y-type arrangements.

	4a (0,0,0)	4c (0.25, 0.25, 0.25)	4b (0.5, 0.5, 0.5)	4d (0.75, 0.75, 0.75)
YI	Sb	V	Sc/Y	Fe
YII	Sb	Sc/Y	V	Fe
YIII	V	Sb	Sc/Y	Fe

under study. The Birch–Murnaghan equation of states was used to fit the energy-volume data. Figure 1 shows that the structural configuration YI has the lowest total energy for both the FeVScSb and FeVYSb Heusler compounds. Hence, the YI structure is more suited to crystallization of FeVScSb and FeVYSb Heuslers, with Fe, V, Sc/Y, and Sb occupying Wyckoff positions 4d (3/4, 3/4, 3/4), 4c (1/4, 1/4, 1/4), 4b (1/2, 1/2, 1/2), and 4a (0, 0, 0), respectively. In Table 2, we summarize the equilibrium lattice constants ( $a_0$ ), equilibrium lattice ( $V_0$ ), bulk modulus ( $B$ ), pressure derivatives ( $B'$ ), and the total energies  $E_{\text{tot}}$ . Lattice constant optimization results in values of 6.34 and 6.64 Å for FeVScSb and

FeVYSb, respectively. When the Z-atomic atom's number grows, the lattice constant rises, suggesting that hybridization between atoms weakens. The optimum lattice parameters of Heusler compounds FeVScSb and FeVYSb accord well with previous theoretical predictions.<sup>[53]</sup> Cohesive and formation energy can be used to investigate the quaternary FeVScSb and FeVYSb Heusler alloys' physicochemical stability

$$E_{\text{coh}} = \frac{1}{4} \left[ E_{\text{Tot}}^{\text{FeV(Sc/Y)Sb}} - \left( E_{\text{atom}}^{\text{Fe}} + E_{\text{atom}}^{\text{V}} + E_{\text{atom}}^{\text{Sc/Y}} + E_{\text{atom}}^{\text{Sb}} \right) \right] \quad (1)$$

$$E_{\text{For}} = \frac{1}{4} \left[ E_{\text{Tot}}^{\text{FeV(Sc/Y)Sb}} - \left( E_{\text{bulk}}^{\text{Fe}} + E_{\text{bulk}}^{\text{V}} + E_{\text{bulk}}^{\text{Sc/Y}} + E_{\text{bulk}}^{\text{Sb}} \right) \right] \quad (2)$$

where  $E_{\text{Tot}}^{\text{FeV(Sc/Y)Sb}}$  is the equilibrium total energy,  $E_{\text{atom}}^{\text{Fe}}$ ,  $E_{\text{atom}}^{\text{V}}$ ,  $E_{\text{atom}}^{\text{Sc/Y}}$ , and  $E_{\text{atom}}^{\text{Sb}}$  are the isolated atomic energies of the elements Fe, V, (Sc/Y), and Sb, respectively, and  $E_{\text{bulk}}^{\text{Fe}}$ ,  $E_{\text{bulk}}^{\text{V}}$ ,  $E_{\text{bulk}}^{\text{Sc/Y}}$ , and  $E_{\text{bulk}}^{\text{Sb}}$  are the equilibrium total energies per atom for bulk Fe, V, (Sc/Y), and Sb, respectively. Cohesion and formation energies have been computed for FeVScSb at  $-0.49$  and  $-5.07$  eV atom<sup>-1</sup>, and for FeVYSb at

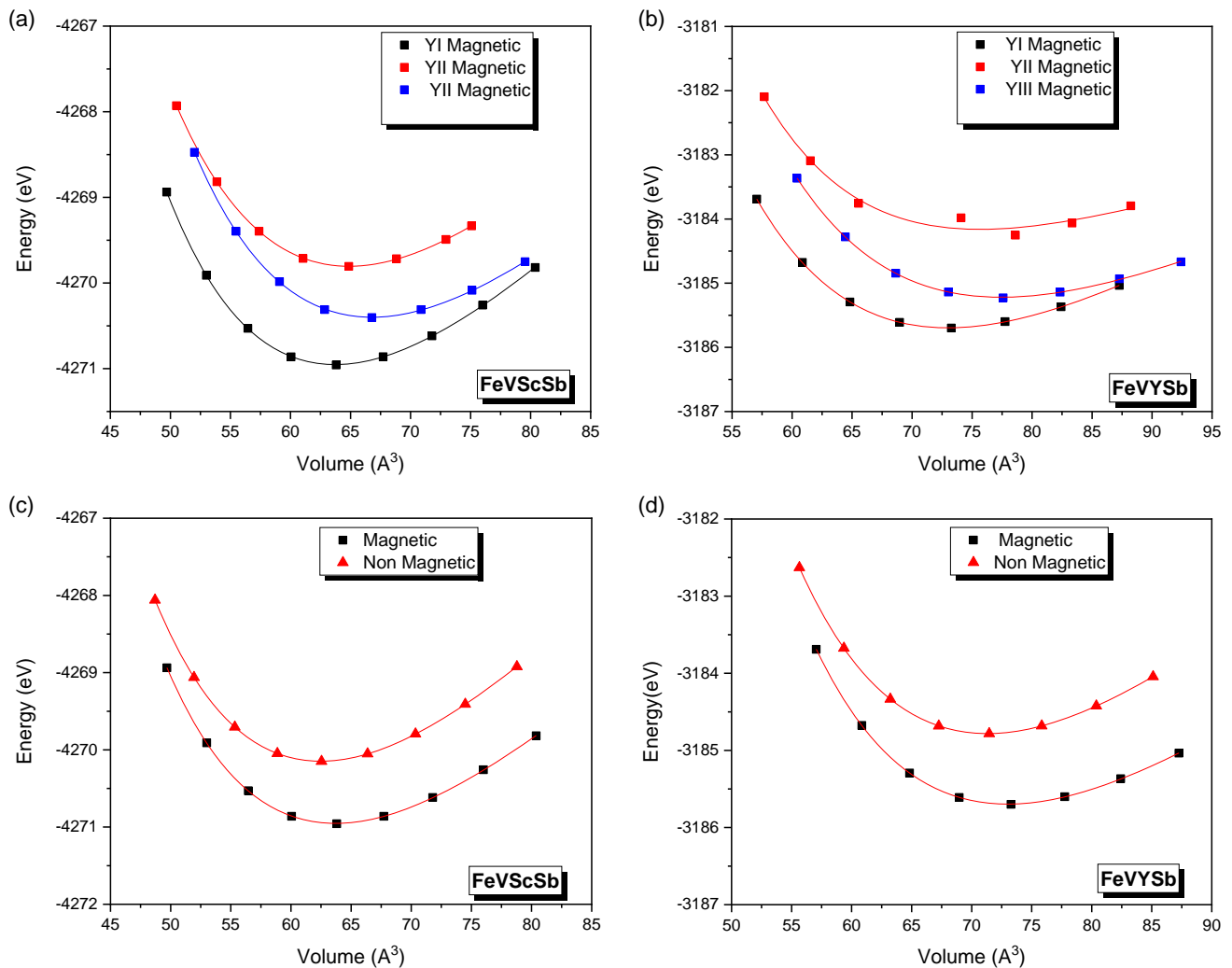


**Figure 1.** Energy versus unit cell volume in the nonmagnetic and magnetic configurations of a,c) FeVScSb and b,d) FeVYSb.

**Table 2.** Calculated equilibrium parameters for FeVScSb and FeVYSb Heusler alloys.

Alloys	$a_0$ [Å]	$V_0$ [Å <sup>3</sup> ]	$B_0$ [GPa]	$B'$	$E_0$ [eV]	$E_{\text{coh}}$ [eV atom <sup>-1</sup> ]	$E_{\text{For}}$ [eV atom <sup>-1</sup> ]
FeVScSb	6.341, 6.342 <sup>[53]</sup>	63.75	130.33	4.77	-4270.95	-5.07	-0.49
FeVYSb	6.640, 6.640 <sup>[53]</sup>	73.18	110.40	5.28	-3185.69	-4.82	-0.21

-0.21 and -4.82 eV atom<sup>-1</sup>, respectively. These two materials are stable and amenable to experimental synthesis, as indicated by the negative numbers. As it has the lowest formation energy, FeVScSb is the easiest to synthesize. In light of these results, further analysis on the electronic, elastic, and magnetic characteristics of FeVScSb and FeVYSb was conducted only on this structure (type I+ ferromagnetic state).

### 3.2. Elastic Properties

The elastic properties of a material are the most precise indicators of its mechanical characteristics. The assessment of a solid's elastic stability involves the consideration of its elastic constants  $C_{ij}$ , which are the macroscopic parameters in a uniform solid that establish the relationship between stress and deformation. This is in addition to the modulus of compressibility  $B$ .<sup>[54]</sup>

The mechanical stability of a cubic system requires only the three independent elastic constants  $C_{11}$ ,  $C_{12}$ , and  $C_{44}$  to obey the following Born condition:<sup>[55]</sup> ( $C_{11} - C_{12}$ ) > 0; ( $C_{11} + 2C_{12}$ ) > 0;  $C_{11} > 0$ ;  $C_{44} > 0$ ; and  $C_{12} < B < C_{11}$ , where the elastic constant  $C_{11}$  reflects the resistance of the crystal to unidirectional compression, and  $C_{12}$  and  $C_{44}$  represent the resistance to shear stress. As the value of the elastic constant  $C_{11}$  is greater than that of  $C_{12}$  and  $C_{44}$ , this suggests that the FeVScSb and FeVYSb Heusler materials are more resistant to shear than they are to compression. We found that FeVScSb and FeVYSb are elastically stable because they obey the Born condition, as shown in Table 3. Some mechanical properties, like bulk modulus  $B$ , shear modulus  $G$ , Young's modulus  $E$ , Poisson's ratio, and universal anisotropy factor  $A^U$ , can be derived from computed elastic constants.<sup>[56]</sup>

$$B = \frac{C_{11} + 2C_{12}}{3} \quad (3)$$

**Table 3.** The obtained elastic parameters of FeVScSb and FeVYSb.

Parameters	FeVScSb	FeVYSb
$C_{11}$	225.89	168.824
$C_{12}$	95.55	71.129
$C_{44}$	86.12	25.009
$B$	138.99	103.694
$G$	77.02	32.809
$B/G$	1.80	3.16
$E$	195.04	89.038
$\Sigma$	0.27	0.36
$\Theta_D$	432.24	269.10
$A^U$	0.09	0.56

$$G_V = \frac{C_{11} - C_{12} + 3C_{44}}{5} \quad (4)$$

$$G_R = \frac{5(C_{11} - C_{12})C_{44}}{3(C_{11} - C_{12}) + 4C_{44}} \quad (5)$$

$$G_H = \frac{G_V + G_R}{2} \quad (6)$$

$$E = \frac{9BG}{3B + G} \quad (7)$$

$$A^U = 5 \frac{G_V}{G_R} + \frac{B_V}{B_R} - 6 \quad (8)$$

$$\sigma = \frac{3B - 2G}{2(3B + G)} \quad (9)$$

The obtained values are also listed in Table 3. The values of the compressibility module obtained from the  $C_{ij}$  are in perfect accord with those obtained by smoothing the ( $E$ - $V$ ) state equations. FeVYSb is less resistant to compression and shear compared to FeVScSb because the  $B = 103.6947$  GPa of FeVYSb is smaller than the  $B = 138.99$  GPa of FeVScSb. Poisson's ratio is used to distinguish the nature of forces between atoms constituting a solid material and, thus, the type of interatomic bonds. For FeVScSb,  $\sigma$  is close to 0.25, which indicates that these materials present a central interatomic interaction or ion crystal, although the value of 0.31 (FeVYSb) is for metallic materials. The Pugh's ratio, abbreviated as  $B/G$ , is a method for determining whether or not a material is brittle (when  $B/G$  is less than 1.75), or ductile (when  $B/G$  is greater than 1.75). It is equivalent to 1.80 and 3.16 for FeVScSb and FeVYSb, respectively. Since then, we know that both FeVScSb and FeVYSb Heusler are ductile, with the caveat that the ductility of the FeVYSb Heusler compound is greater than that of the FeVScSb Heusler compound. The Debye temperature ( $\Theta_D$ ) is correlated with thermal and elastic characteristics. It equals 432.24 K for Heuslers composed of FeVScSb and 269.10 K for those composed of FeVYSb. The values of the anisotropy coefficient were found  $A^U \neq 0$  for the two compounds, thus indicating that they are elastically anisotropic, and it shows that FeVScSb is less elastically anisotropic compared to FeVYSb.

The preceding investigation was insufficient in delineating the elastic properties of the crystal. Prioritizing the utilization of surface structures that exhibit the directional reciprocal of Young's modulus is a recommended approach for practical applications. According to Ref. [57], it is possible to depict the distribution of  $E$  in a cubic material through 3D polar illustrations.

$$E = \frac{1}{S_{11} - 2(S_{11} - S_{12} - \frac{1}{2}S_{44})(n_1^2n_2^2 + n_2^2n_3^2 + n_3^2n_1^2)} \quad (10)$$



$S_{ij}$  are the deformability elastic constants,  $n_1 = \sin \theta \cos \varphi$ ,  $n_2 = \sin \theta \sin \varphi$ , and  $n_3 = \cos \theta$ . **Figure 2** shows how the projected orientation effects on Young's modulus behave for FeVScSb and FeVYSb. If the system were entirely isotropic in all directions, the surface here would assume the form of a sphere. Nevertheless, neither of these items is accurate; neither the FeVScSb nor the FeVYSb Young's modulus surfaces can be described as spherical in any way. As compared to FeVScSb, which has nearly isotropic behavior, we found that FeVYSb exhibited anisotropy on a wide scale caused by differences in bonding characteristics between adjacent atomic planes. This was seen in contrast to the nearly isotropic behavior of FeVScSb. The anisotropy of the elastic properties of FeVScSb is practically the same in the plane ( $X=Y$ ) as it is in the ( $XY$ ), ( $XZ$ ), and ( $YZ$ ) planes, as well as the Young modulus's surface being almost spherical. Alternatively, the anisotropy in the ( $XY$ ), ( $XZ$ ), and ( $YZ$ ) planes of FeVYSb is greater than that of the ( $XY$ ) plane. As a consequence of our research, we have found that the compound with the highest level of anisotropy is FeVYSb, whereas the compound with the lowest level of anisotropy is FeVScSb.

### 3.3. Electronic and Magnetic Properties

Electronic, optical, transport, and magnetic characteristics are only a few of the many essential physical ones that may be accessible from the band structure of solids. **Figure 3** displays the zero-pressure majority- and minority-spin band structures of FeVScSb and FeVYSb compounds. Galanakis et al.<sup>[16]</sup> established a naming convention for the irreducible representations of the spin-up/down states at the point  $\Gamma$  for  $s$ -bands, which is 1, for  $p$ -bands, which is 3, for  $e$ -bands, which is 2, and for  $t$ -bands, which is 3. The  $e$ - and  $t$ -bands are formed when  $3d$  ( $4d$ ) orbitals of Fe, V, (Y), and Sc atoms hybridize with one another.

The Heusler compounds FeVScSb (as shown in Figure 3a) and FeVYSb (as shown in Figure 3c) both demonstrate semiconductor properties in the spin-up direction, with direct bandgaps of 0.56 and 0.30 eV, respectively. This is due to the positioning of the Fermi level ( $E_F$ ) between the fully occupied valence bands  $s$ ,  $p$ ,  $2e_g$ ,  $3t_{2g}$ , and  $3t_{1u}$ , and the unoccupied conduction bands  $2e_u$ . The spin-down band structures of FeVScSb (as shown in Figure 3b) and FeVYSb (as shown in Figure 3d) exhibit a

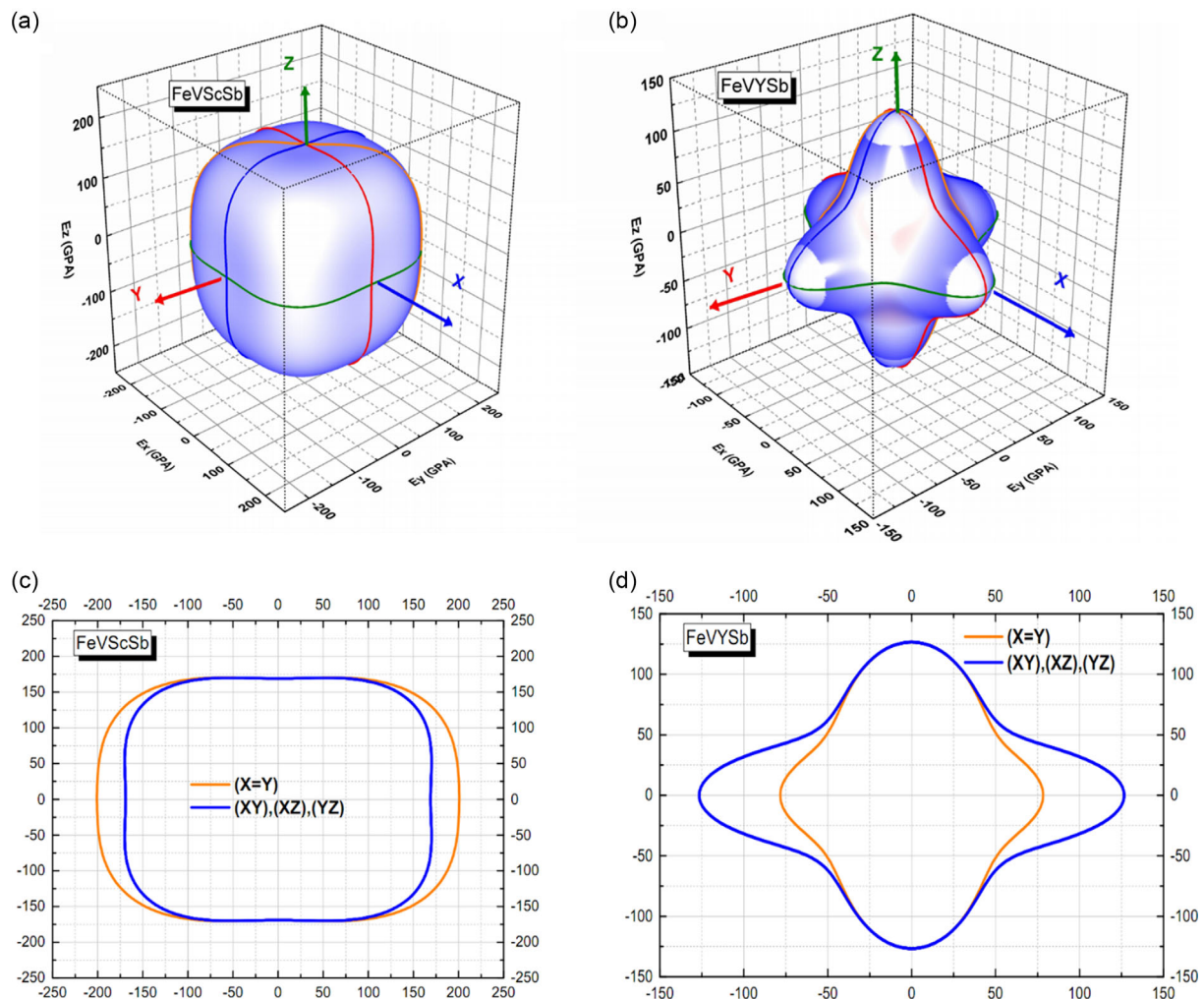


**Figure 2.** 3D surfaces of Young's modulus for a) FeVScSb, b) FeVScSb, and c,d) their plane-specific cross sections.

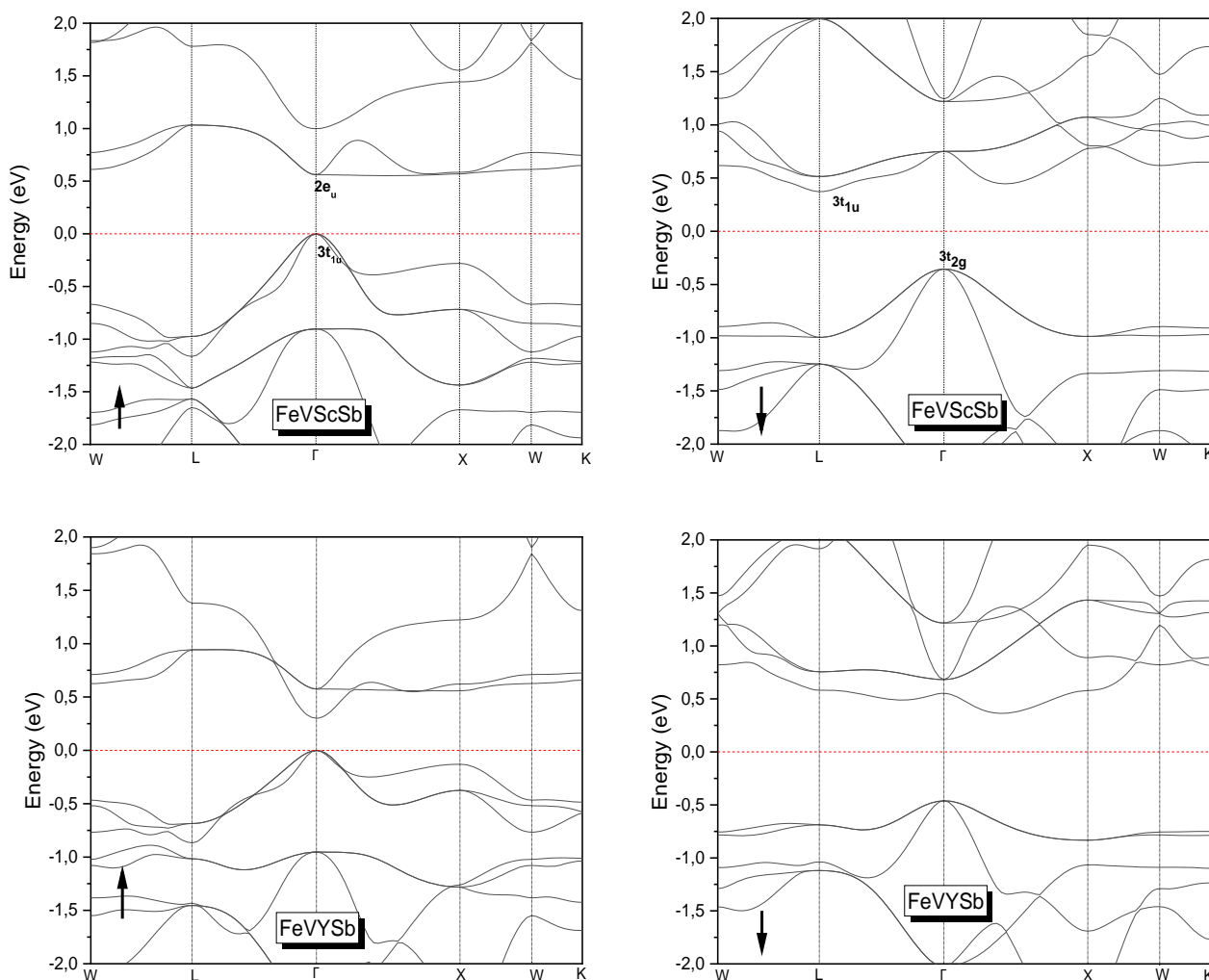


**Figure 3.** Band structure of FeVScSb and FeVYSb at their equilibrium lattice.

semiconductor behavior, with the Fermi level situated between the occupied valence bands ( $s$ ,  $p$ ,  $2e_g$ , and  $3t_{2g}$ ) and the unoccupied conduction bands ( $3t_{1u}$ ). The indirect bandgap  $\Gamma$ -L ( $\Gamma \rightarrow \Gamma$ -X) for FeVScSb and FeVYSb is 0.73 and 0.83 eV, respectively.

Thus, in the case of FeVScSb (FeVYSb), it can be observed that the L ( $\Gamma$ -X) direction, which represents the highest symmetry point, is associated with the lowest energy level of the  $3t_{1u}$  conduction band. On the other hand, the highest energy level of the  $3t_{2g}$  valence band is represented by the highest symmetry point  $\Gamma$ . With respect to the two spin orientations, it can be observed that both of our alloys exhibit magnetic semiconductor properties at a pressure of 0 GPa.

The state densities for FeVScSb and FeVYSb Heuslers at 0 GPa are presented in **Figure 4**, encompassing both total and partial values. The total density of states (DOS) structure of our compounds exhibits a notable similarity. The findings depicted in Figure 4 indicate that the magnetic moments of the transition elements (Fe, V, Sc, and Y) are predominantly attributed to the  $d$  states, whereas the magnetic moments of the Sb atom are attributed to the  $s$ - $p$  states. The discernible

energy distance between the  $s$  and  $p$  states of the antimony atom and the  $d$  states of the iron, vanadium, scandium, and yttrium atoms is evident. The hybridization of  $d$  orbitals in Fe, V, Sb, and Y atoms is evident, resulting in the division of bonding e.g., and  $t_{2g}$  orbitals (situated below the Fermi level), nonbonding  $e_u$  and  $t_{1u}$  orbitals (around the Fermi level), and antibonding e.g., and  $t_{2g}$  orbitals (positioned above the Fermi level). The  $d$ - $d$  bandgap is a type of bandgap that arises due to the hybridization of  $d$ - $d$  orbitals in transition metals. The bandgap in  $\text{AlCu}_2\text{Mn}$  full-Heusler alloys is attributed to the  $d$ - $d$  bandgap. The hybridization between the  $d$  states of Fe, V, Sc, and Y and the  $p$  states of Sb governs the degree of occupancy of the  $p$ - $d$  orbital. The hybridization process induces a modification in the magnitude of the energy gap. The majority of electronic states that exist at the Fermi level  $E_F$  within transition metals, such as Fe, V, (Y), and Sc, are a result of hybridization between  $3d$  ( $4d$ ) orbitals. There exist three plausible hypotheses regarding the origin of the bandgap in HM. The three phenomena under consideration are as follows: 1) the bandgap resulting from  $d$ - $d$  hybridization, as depicted in **Figure 5**, 2) charge transfer, and 3) the presence of a

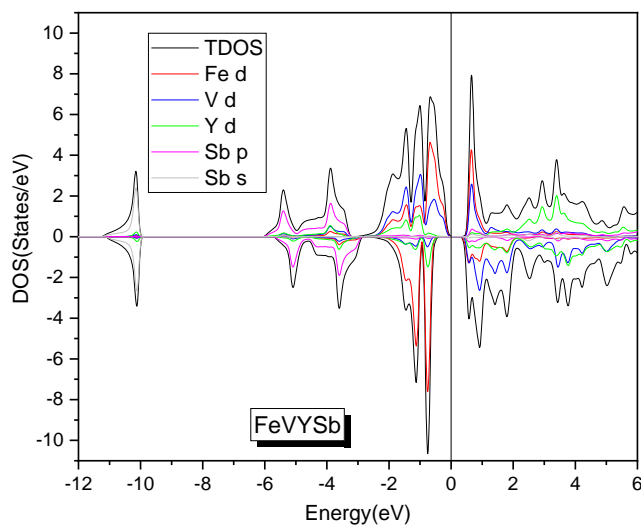
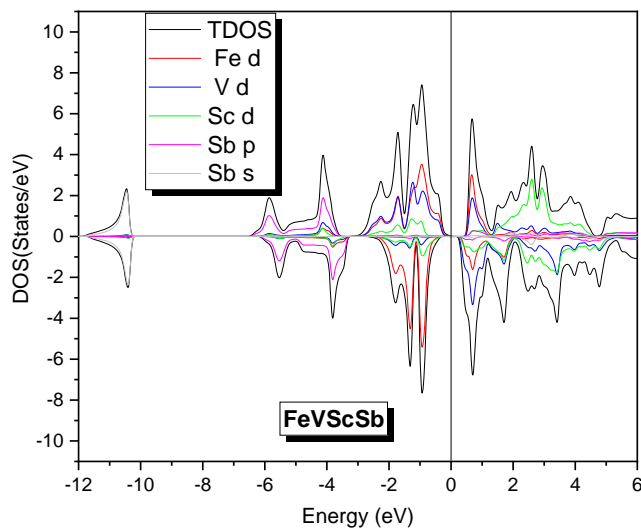


**Figure 4.** The total and partial state densities of FeVScSb and FeVYSb in type I as determined by GGA.

covalent band. In this study, the origin of the bandgap in these compounds is investigated by examining the hybridization of *d*-electrons among the transition metals. The bandgap of said complexes was ascertained through the observation of *d* electron hybridization between transition metal constituents, thereby determining its origin. Magnetic semiconductors exhibit discontinuous energy bands owing to their dual characteristics as both semiconductors and magnets. The Generalized Slater–Pauling law<sup>[40,58]</sup> predicts that Heusler compounds containing 21 valence electrons will display a split energy band at the Fermi energy. Figure 5 depicts the schematic representation of the electronic band structures for both majority and minority spin in semiconductors possessing 21 valence electrons. The determination of the hybridization process can be ascertained by following the criteria outlined in reference number 60. The *s*-*p* atom generates a single *s*-band and three *p*-bands.

The *d*-orbitals of the  $X_A$  and  $X'_C$  atoms then combine to form a hybrid. When this happens, the hybridized orbital begins

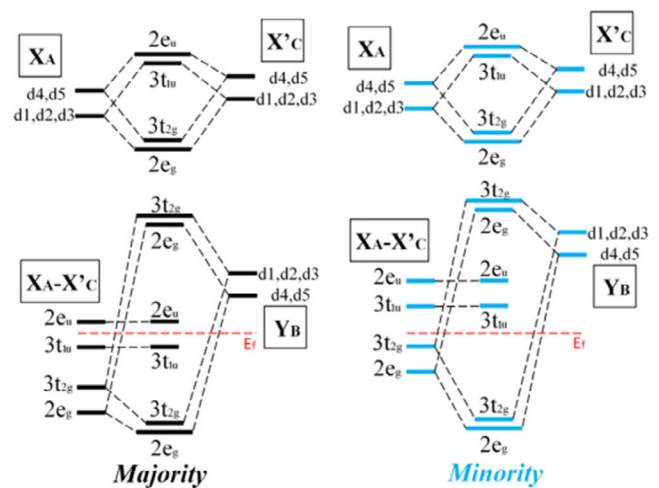


**Figure 5.** Diagram depicting the majority–minority gap's origins in FeVScSb and FeVYSb.

coupling with the  $Y_B$  atom's *d*-orbital. A single *s*-band, three *p*-bands, double-degenerated  $e_g$ , triple-degenerated  $t_{2g}$ , and a single  $t_{1u}$  will be seen when hybridization is complete. One *s*-band state, three *p*-band states, and eight *d*-band states are possible in a single atom. Heusler compounds usually contain a total of 21 valence electrons, with 12 of them being valence electrons that can be fully utilized. However, it is noteworthy that the minority spin energy band has only nine valence electrons, resulting in the  $t_{1u}$  orbital being unoccupied. The presence of dissymmetry results in the manifestation of magnetism and a bandgap. Theoretically, it is expected that Heusler compounds possessing 21 valence electrons would exhibit magnetic semiconductor behavior. The disparity in spin energy between hybrid orbitals  $t_{1u}$  and  $e_u$ , as illustrated in Figure 5, is exclusively governed by the atoms occupying the A and C sites. The impact of A site and C site atoms on the spin energy gaps between hybrid orbitals  $t_{1u}$  and  $t_{2g}$  is noteworthy. Thus, the atoms occupying the A and C sites play a crucial role in determining the energy band in proximity to the Fermi level. If the B site and D site elements are modified while keeping the valence electrons unchanged, the energy band is expected to undergo a minor shift.

In order to investigate the impact of strain on physical characteristics, the latter were estimated utilizing the subsequent correlation

$$\varepsilon(\%) = \frac{a - a_0}{a_0} \times 100 \quad (11)$$

where  $a_0$  is the the optimized lattice parameter, and  $a$  is the lattice parameter that exhibits strain.

The present study involves the computation of spin-polarized electronic band structures of FeVScSb and FeVYSb Heusler compounds under varying degrees of strain, ranging from −8% to 7% for FeVScSb and from −8% to 3% for FeVYSb. The objective of this investigation is to assess the robustness of the electronic structure in response to strain-induced effects. The present study illustrates the shift of the lowest  $3t_{2g}$  ( $2e_u$ ) and highest  $2e_g$  ( $3t_{1u}$ ) bands along the spin-up (down) direction under strain for

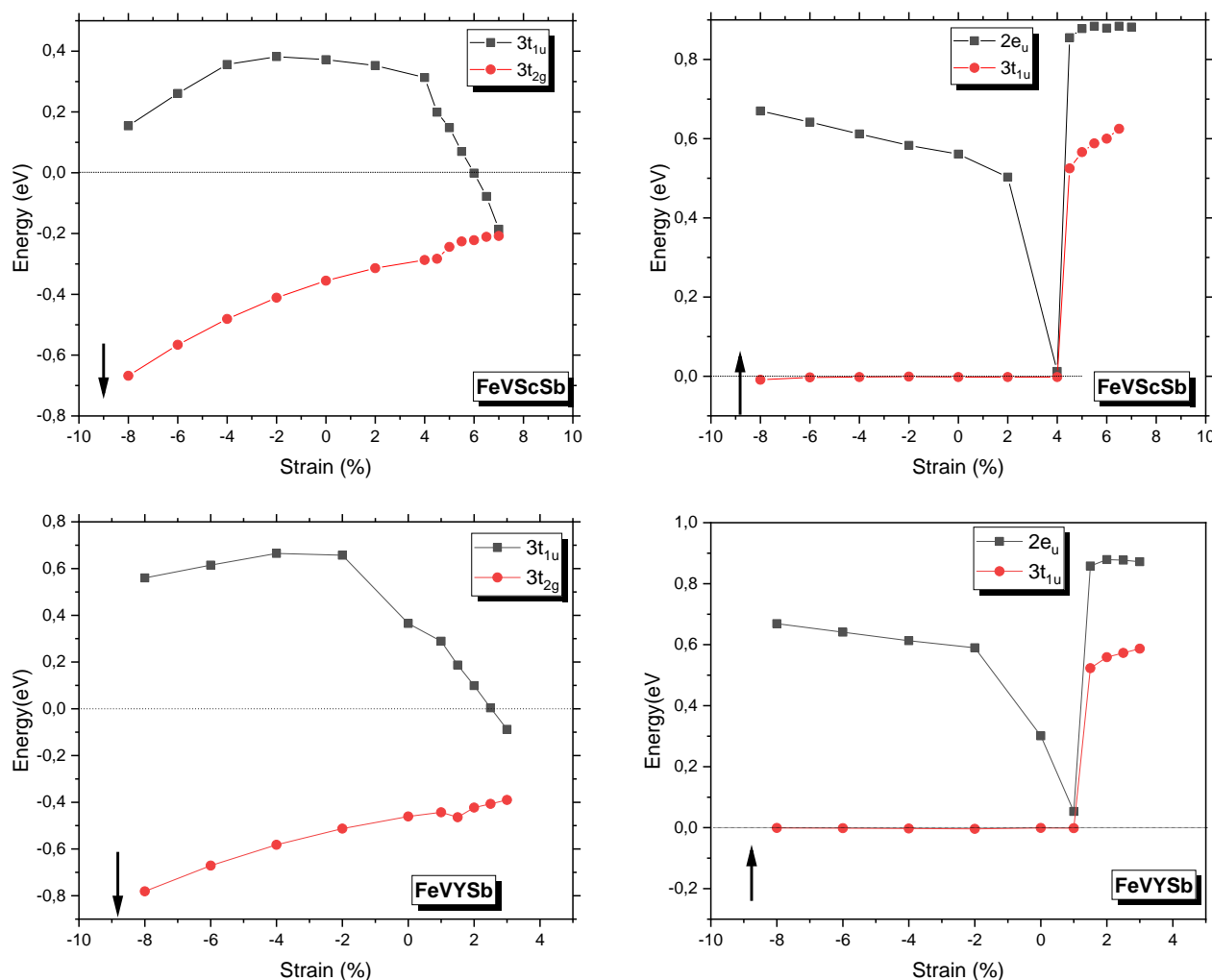


**Figure 6.** Strain impact on the minima of the  $2e_u$  and  $3t_{1u}$  conduction bands and the maxima of  $3t_{1u}$  and  $3t_{2g}$  valence bands of FeVScSb and FeVYSb.

FeVScSb and FeVYSb Heusler materials, as depicted in Figure 6a (Figure 6c) and Figure 6b (Figure 6d), respectively. The findings of our study indicate that the semiconductivity of alloys remains consistent across a broad spectrum of lattice parameters, ranging from 5.84 to 6.60 Å for FeVScSb, and from 6.11 to 6.70 Å for FeVYSb. The Heusler compounds FeVScSb and FeVYSb exhibit half-metallic behavior within a specific range of lattice parameters. Specifically, FeVScSb displays half-metallicity when the lattice parameter varies from 6.61 to 6.72 Å, while FeVYSb exhibits this behavior within the range of 6.71 to 6.81 Å. The research findings indicate that the spin-up energy bandgap of Heusler compounds FeVScSb and FeVYSb exhibits a decreasing trend as the lattice parameters increase.

The Hirshfeld electron populations were analyzed to estimate the total and partial magnetic moments of FeVScSb and FeVYSb. Figure 7 illustrates the progression of their development in relation to the applied strain. The study revealed that the  $m_{\text{tot}}$  values of FeVScSb and FeVYSb were determined to be  $3 \mu_B$ , and were found to conform to the Slater–Pauling rule, as denoted by the subsequent equation: The equation  $M_T = Z_T - 2n_d$  is given,

where  $Z_T$  is equal to 21 and  $n_d$  is equal to 9. Table 4 illustrates the alterations in the complete and partial magnetic moments of FeVScSb and FeVYSb substances under the influence of strain. Upon computing the magnetic moment at the equilibrium lattice constant, it is evident that the dominant contributor is V, exhibiting a magnitude of  $2.40 \mu_B$  for FeVScSb and  $2.66 \mu_B$  for FeVYSb. The magnetic moments of V, Sc, and Sb atoms exhibit an increase with an increase in lattice parameters, while the magnetic moment of Fe atom experiences a decrease with an increase in lattice parameters, yet it remains constant at  $3 \mu_B$ .

## 4. Conclusion

The present study offers a theoretical examination of the influence of strain on the structural, elastic, electronic, and magnetic characteristics of the FeVScSb and FeVYSb Heusler alloys. The ultrasoft pseudopotential method, as implemented in the CASTEP software, was utilized to perform the calculations. The results of the geometry optimization indicate that the FeVScSb and FeVYSb materials exhibit stability and form



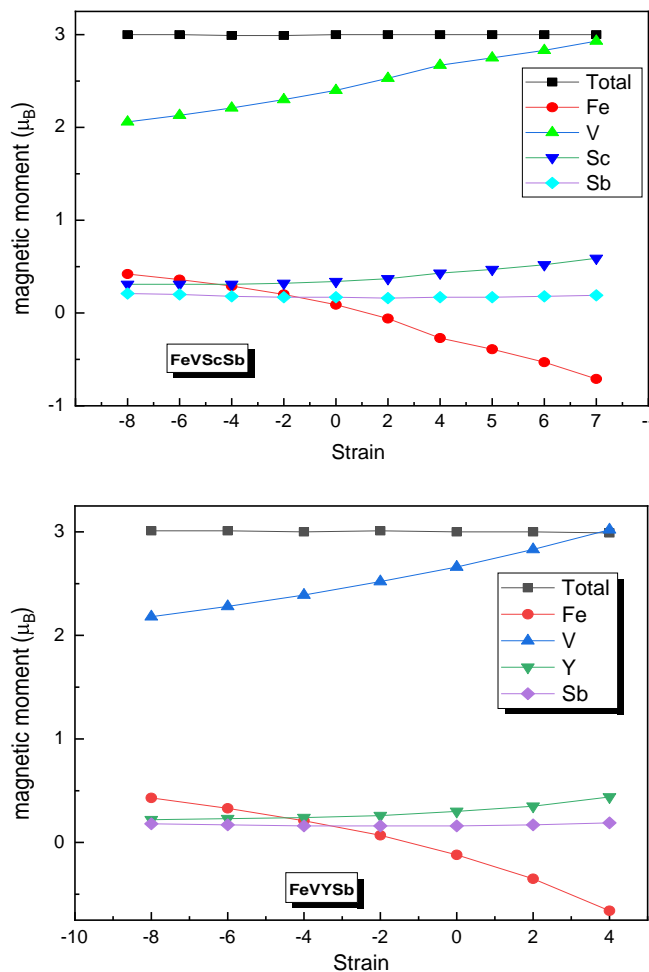


**Figure 7.** Strain-dependent magnetic moments for FeVScSb and FeVYSb.

crystals with a YI structure that is ferromagnetic. Specifically, the Fe, V, Sc/Y, and Sb atoms are situated at 4d, 4c, 4b, and 4a positions, respectively. The lattice constant acquired exhibits a satisfactory level of agreement with the existing literature. The elastic constants ( $C_{ij}$ ) computations indicate that the Heusler compounds FeVScSb and FeVYSb possess higher resistance to uniaxial strain in comparison to shear deformation. Furthermore, these compounds are deemed stable and ductile.

The semiconductor behavior of FeVScSb and FeVYSb is observed across a broad spectrum of lattice parameters, as inferred from the analysis of their electronic structure. FeVScSb and FeVYSb exhibit semiconductor properties within distinct lattice parameter ranges, namely, 5.84–6.60 Å and 6.11–6.70 Å, respectively. The FeVScSb and FeVYSb Heusler compounds display half-metallic characteristics with considerable spin polarization upon alteration of their lattice parameter. The observed phenomenon is attributed to FeVScSb and FeVYSb materials, respectively, in response to changes in the lattice parameter. Specifically, FeVScSb exhibits this behavior within the range of 6.61–6.72 Å, whereas FeVYSb displays it within the range of 6.71–6.81 Å. The magnetic moment of  $3\mu_B$  is

**Table 4.** The calculated magnetic moments,  $m_{\text{tot}}$ ,  $m_{\text{Fe}}$ ,  $m_{\text{V}}$ ,  $m_{\text{Y}}$ ,  $m_{\text{Sb}}$  in  $\mu_B$ ,  $E_{\text{HM}}$ , and  $E_{\text{SC}}$  bandgaps in eV for half-metal semiconductor, respectively, and polarization in %.

Compounds	Strain	A	$m_{\text{tot}}$	$m_{\text{Fe}}$	$m_{\text{V}}$	$m_{\text{Y}}$	$m_{\text{Sb}}$	$E_{\text{HM}}$	$E_{\text{SC}}$	P%
FeVScSb	−8	5.84	3.00	0.42	2.06	0.31	0.21	−	0.15	−
	−6	5.96	3.00	0.36	2.13	0.31	0.20	−	0.25	−
	−4%	6.09	2.99	0.29	2.21	0.31	0.18	−	0.34	−
	−2%	6.22	2.99	0.20	2.30	0.32	0.17	−	0.38	−
	0%	6.341	3.00	0.09	2.40	0.34	0.17	−	0.37	−
	2%	6.47	3.00	−0.06	2.53	0.37	0.16	−	0.35	−
	4%	6.60	3.00	−0.27	2.67	0.43	0.17	−	0.01	−
	4.5%	6.63	3.00	−0.33	2.71	0.45	0.17	0.49	−	100
	5%	6.66	3.00	−0.39	2.75	0.47	0.17	0.39	−	100
	5.5%	6.69	3.00	−0.46	2.79	0.49	0.18	0.30	−	100
	−8	6.11	3.01	0.43	2.18	0.22	0.18	−	0.56	−
	−6	6.24	3.01	0.33	2.28	0.23	0.17	−	0.61	−
FeVYSb	−4%	6.38	3.00	0.21	2.39	0.24	0.16	−	0.60	−
	−2%	6.51	3.01	0.07	2.52	0.26	0.16	−	0.50	−
	0%	6.64	3.00	−0.12	2.66	0.30	0.16	−	0.30	−
	1%	6.71	2.99	−0.23	2.74	0.32	0.16	−	0.053	−
	1.5%	6.74	3.00	−0.29	2.79	0.34	0.16	0.651	−	100
	2%	6.77	3.00	−0.35	2.83	0.35	0.17	0.52	−	100
	2.5%	6.81	3.00	−0.42	2.88	0.37	0.17	0.41	−	100

retained by the FeVScSb and FeVYSb Heusler compounds over the range of strain investigated. As a result, these chemical compounds have been acknowledged as a viable alternative for utilization in magnetic tunnel junctions and spin valves, due to their significant spin polarization, as observed from a spintronics perspective.

## Acknowledgements

The authors (I.B., H.B., T.G., and Z.C.) would like to express gratitude to the General Directorate for Scientific Research and Technological Development for the financial assistance they provided over the course of this work's execution.

## Conflict of Interest

The authors declare no conflict of interest.

## Data Availability Statement

The data that support the findings of this study are available from the corresponding author upon reasonable request.

## Keywords

magnetic semiconductors, quaternary compounds, role of strain

Received: April 13, 2023  
Revised: June 1, 2023  
Published online:

- [1] I. Žutić, J. Fabian, S. D. Sarma, *Rev. Mod. Phys.* **2004**, 76, 323.
- [2] C. Felser, G. H. Fecher, B. Balke, *Angew. Chem. Int. Ed.* **2007**, 46, 668.
- [3] H. Ohno, *Nat. Mater.* **2010**, 9, 952.
- [4] J. Kübler, G. H. Fecher, C. Felser, *Phys. Rev. B* **2007**, 76, 024414.
- [5] L. Bainsla, K. G. Suresh, A. K. Nigam, M. M. Raja, B. S. D. C. S. Varaprasad, Y. K. Takahashi, K. Hono, *J. Appl. Phys.* **2014**, 116, 203902.
- [6] L. Bainsla, A. I. Mallick, A. A. Coelho, A. K. Nigam, B. S. D. C. S. Varaprasad, Y. K. Takahashi, A. Alam, K. G. Suresh, K. Hono, *J. Magn. Magn. Mater.* **2015**, 394, 82.
- [7] K. Özdoğan, B. Aktaş, I. Galanakis, E. Şaşıoğlu, *J. Appl. Phys.* **2007**, 101, 073910.
- [8] R. A. de-Groot, F. M. Mueller, P. G. van Engen, K. H. J. Buschow, *Phys. Rev. Lett.* **1983**, 50, 2024.
- [9] G. D. Liu, X. F. Dai, H. Y. Liu, J. L. Chen, Y. X. Li, G. Xiao, G. H. Wu, *Phys. Rev. B* **2008**, 77, 014424.
- [10] I. Galanakis, K. Özdoğan, E. Şaşıoğlu, B. Aktaş, *Phys. Rev. B* **2007**, 75, 172405.
- [11] P. Lukashev, P. Kharel, S. Gilbert, B. Staten, N. Hurley, R. Fuglsby, Y. Huh, S. Valloppilly, W. Zhang, K. Yang, R. Skomski, D. J. Sellmyer, *Appl. Phys. Lett.* **2016**, 108, 141901.
- [12] I. Galanakis, E. Şaşıoğlu, *Appl. Phys. Lett.* **2011**, 99, 052509.
- [13] J. Li, Y. Li, G. Zhou, Y. Sun, C. Q. Sun, *Appl. Phys. Lett.* **2009**, 94, 242502.
- [14] I. Galanakis, P. Mavropoulos, P. H. Dederichs, *J. Phys. D: Appl. Phys.* **2006**, 39, 765.
- [15] S. Skaftouros, K. Özdoğan, E. Şaşıoğlu, I. Galanakis, *Phys. Rev. B* **2013**, 87, 024420.
- [16] I. Galanakis, P. H. Dederichs, N. Papanikolaou, *Phys. Rev. B* **2002**, 66, 174429.
- [17] I. Galanakis, P. H. Dederichs, N. Papanikolaou, *Phys. Rev. B* **2002**, 66, 134428.
- [18] M. J. Carey, T. Block, B. A. Gurney, *Appl. Phys. Lett.* **2004**, 85, 4442.
- [19] T. Block, M. J. Carey, B. A. Gurney, O. Jepsen, *Phys. Rev. B* **2004**, 70, 205114.
- [20] I. Galanakis, E. Şaşıoğlu, *J. Phys. D: Appl. Phys.* **2011**, 44, 235001.
- [21] A. Ayuela, J. Enkovaara, K. Ullakko, R. M. Nieminen, *J. Phys.: Condens. Matter* **1999**, 11, 2017.
- [22] V. V. Godlevsky, K. M. Rabe, *Phys. Rev. B* **2001**, 63, 134407.
- [23] J. Drews, U. Eberz, H. Schuster, *J. Less-Common Met.* **1986**, 116, 271.
- [24] X. Dai, G. Liu, G. H. Fecher, C. Felser, Y. Li, H. Liu, *J. Appl. Phys.* **2009**, 105, 07E901.
- [25] J. Kudrnovský, V. Drchal, S. K. Bose, I. Turek, *Phys. Rev. B* **2018**, 97, 214404.
- [26] V. Alijani, M. J. E. Richardson, *Phys. Rev. B* **2011**, 84, 224416.
- [27] P. Klaer, B. Balke, V. Alijani, J. Winterlik, G. H. Fecher, C. Felser, H. J. Elmers, *Phys. Rev. B* **2011**, 84, 144413.
- [28] L. Bainsla, A. I. Mallick, M. M. Raja, A. K. Nigam, B. S. D. C. S. Varaprasad, Y. K. Takahashi, A. Alam, K. G. Suresh, K. Hono, *Phys. Rev. B* **2015**, 91, 104408.
- [29] Y. Feng, H. Chen, H. Yuan, Y. Zhou, X. Chen, *J. Magn. Magn. Mater.* **2015**, 378, 7.
- [30] K. Özdoğan, E. Şaşıoğlu, I. Galanakis, *J. Appl. Phys.* **2013**, 113, 193903.
- [31] G. Y. Gao, L. Hu, K. L. Yao, B. Luo, N. Liu, *J. Alloys Compd.* **2013**, 551, 539.
- [32] A. Kundu, S. Ghosh, R. Banerjee, S. Ghosh, B. Sanyal, *Sci. Rep.* **2017**, 7, 1803.
- [33] P. L. Yan, J. M. Zhang, B. Zhou, K. W. Xu, *J. Phys. D: Appl. Phys.* **2016**, 49, 255002.
- [34] P. Wang, J. B. Xia, W. Zhongming, H. Wen, X. Zong, H. B. Wu, *J. Appl. Phys.* **2019**, 52, 505003.
- [35] R. B. Ray, G. C. Kaphle, R. K. Rai, D. K. Yadav, R. Paudel, D. Paudyal, *J. Alloys Compd.* **2021**, 867, 158906.
- [36] L. Xiong, L. Yi, G. Y. Gao, L. Xiong, *J. Magn. Magn. Mater.* **2014**, 360, 98.
- [37] M. Rahmoune, A. Chahed, A. Amar, H. Rozale, A. Lakdja, O. Benhelal, A. Sayede, *Mater. Sci.* **2016**, 34, 905.
- [38] W. Kohn, L. J. Sham, *Phys. Rev.* **1965**, 140, A1133.
- [39] S. J. Clark, M. D. Segall, C. J. Pickard, P. J. Hasnip, M. I. Probert, K. Refson, M. C. Payne, *Z. Kristallogr. Cryst. Mater.* **2005**, 220, 567.
- [40] J. P. Perdew, K. Burke, M. Ernzerhof, *Phys. Rev. Lett.* **1996**, 77, 3865.
- [41] D. Vanderbilt, *Phys. Rev. B* **1990**, 41, 7892.
- [42] H. J. Monkhorst, J. D. Pack, *Phys. Rev. B* **1976**, 13, 5188.
- [43] T. H. Fischer, J. Almlof, *J. Phys. Chem.* **1992**, 96, 9768.
- [44] V. Milman, M. C. Warren, *J. Phys.: Condens. Matter* **2001**, 13, 241.
- [45] W. Voigt, in *Lehrbuch der Kristallphysik*, Teubner, Leipzig **1928**.
- [46] A. Reuß, *Angew. Math. Mech.* **1929**, 9, 49.
- [47] R. Hill, *Proc. Phys. Soc. A* **1952**, 65, 349.
- [48] M. A. Zagrebin, V. V. Sokolovskiy, V. D. Buchelnikov, M. A. Klyuchnikova, *Phys. Proc.* **2015**, 75, 1427.
- [49] Z. Charifi, T. Ghellab, H. Baaziz, F. Soyalep, *Int. J. Energy Res.* **2022**, 1.
- [50] Q. Gao, I. Opahle, H. Zhang, *Phys. Rev. Mater.* **2019**, 3, 024410.
- [51] Y. Feng, X. Xu, W. Cao, T. Zhou, *Comput. Mater. Sci.* **2018**, 147, 251.
- [52] H. Baaziz, T. Ghellab, E. Güler, Z. Charifi, Ş. Uğur, M. Güler, G. Uğur, *J. Supercond. Nov. Magn.* **2022**, 35, 1173.
- [53] Y. Wang, Z. Xiaoming, B. Dinga, H. Houa, E. Liua, L. Zhongyuan, X. Xia, H. Zhanga, G. Wua, W. Wanga, *Comput. Mater. Sci.* **2018**, 150, 321.
- [54] C. Kittel, *State Physics*, 7th ed., John Wiley & Sons, New York **1996**, pp. 117–126.
- [55] M. Born, K. Huang, *Dynamic Theory of Crystal*, Clarendon, Oxford **1956**.
- [56] M. Jamal, S. Jalali Asadabadi, I. Ahmad, H. A. Rahnamaye Aliabad, *Comput. Mater. Sci.* **2014**, 95, 592.
- [57] J. F. Nye, *Properties of Crystals* Oxford University Press, New York **1985**.
- [58] I. Galanakis, P. Dederichs, N. Papanikolaou, *Phys. Rev. B* **2002**, 66, 174429.